International Journal of Impact Engineering 150 (2021) 103801

Contents lists available at ScienceDirect

International Journal of Impact Engineering

journal homepage: www.elsevier.com/locate/ijimpeng

Particle surface effects on the spall strength of particle-reinforced polymer matrix composites

Anton Lebar, Rafaela Aguiar, Andrew Oddy, Oren E. Petel *

Department of Mechanical and Aerospace Engineering, Carleton University, 1125 Colonel By Dr, Ottawa, ON K1S 5B6, Canada

ARTICLE INFO

Keywords:
Spall
Plate impact
Polymer matrix composites
Polyurethane
Alumina
Functionalization
Morphology

ABSTRACT

Prior research has observed that the presence of secondary phases in metal alloys influence the failure behaviour of the bulk material, a response which varies based on secondary phase morphology and adhesion to the matrix material. Particle-reinforced polymer composites offer a material system in which variations in adhesion between the sub-phase and polymer matrix can be manipulated with relative ease. In the present study, we investigate the influence of both the particle morphology and matrix-particle interface adhesion on the spall strength of particle-reinforced polymer composites. Adhesion control was achieved using a adhesion-impeding silane treatment of the surface of micron-sized alumina particles. The composites were characterized based on their dynamic tensile (spall) failure strengths. The results showed that while particle morphology effects were minimal, the loss of surface adhesion resulted in a drastic reduction in spall strength. Fractography performed on the fracture surface of the recovered samples showed evidence of poor wetting in the silane-treated composites, confirming the role of particle adhesion in moderating this failure mode.

1. Introduction

Polymer-matrix composites have been used increasingly in applications that require high stiffness and strength on a mass-normalized basis [1,2]. As polymer-reinforced composite panels are commonly compressed at high strain rates in ballistic applications, a number of studies have previously investigated shock wave propagation and delaminations of these polymer-matrix composite materials [3–7]. Optimizing the polymer matrix of those composites through particle reinforcements have been suggested as a means of improving their performance [8]. The shock wave propagation and shear characteristics of alumina-reinforced epoxy have been studied extensively using various techniques [9–15], however the role of these particulate on the dynamic tensile strength of these composites have not been thoroughly investigated. In the present study, we investigate the dynamic tensile failure (spall strength) of a particle-reinforced polymer-matrix composite, specifically focusing on the role of surface adhesion on the failure behaviour of these materials.

Spall is the dynamic tensile failure of a material, which is determined through the rapid compression and subsequent expansion of a specimen. Research into the spall strength and tensile failure mechanisms of metals has spanned several decades [16–18], studying the implications of a range of material properties and experimental parameters including strain rate [19,20], loading wave profile [16,21], micro-structure [22,23], and the presence of secondary phases [24,25]. In the case of armour grade aluminum alloys, intermetallic secondary phases were deliberately introduced through tailored manufacturing processes and were found to reduce the spall strength of the alloy [25]. Specifically, there was evidence of spall failure originating at the phase boundaries. Earlier work found that the spall plane tends to propagate between these inclusions, with cracks initiating or terminating at phase boundaries [26]. Similar work in steels found that cracks clearly nucleated at the phase interfaces, then propagated along the interface or through the brittle secondary phase [27]. Steel specimens with an increased interface density saw a reduced spall strength that was attributed to the higher density of nucleation sites.

Similar observations have been made in metal-matrix composites, with reductions in spall strength correlating with increasing filler volume fraction [28]. It was also observed that the aluminum-alumina (Al-Al_2O_3) composite possessed a higher spall strength relative to other comparable aluminum-ceramic composites, a result attributed to a relatively strong interface adhesion between the aluminum and alumina [28]. In contrast, for a metal-metal composite (Cu/Nb), no difference in spall strength was observed when compared to the as-received copper,

* Corresponding author.
E-mail address: oren.petel@carleton.ca (O.E. Petel).

https://doi.org/10.1016/j.ijimpeng.2020.103801
Received 29 June 2020; Received in revised form 23 October 2020; Accepted 10 December 2020
Available online 17 December 2020

which was attributed to comparable phase stiffnesses [29]. This shows the competing effects of impedance mismatches within the composites and the strength of surface adhesion in controlling failure nucleation.

In polymers, the spall strength is also highly correlated to the microstructure of the polymer. Pepper et al. [30] observed that the spall strength of an epoxy based on the choice of curing agent showed up to 50% improvements due to increased cross-linking of the polymer chains. The addition of carbon nanotubes (CNT) to that same epoxy to create an CNT-epoxy composite resulted in a notable reduction in spall strength in a study by Huneault et al. [31]. Bie et al. [32] studied a similar CNT-epoxy composite system and found that the spall strength of the neat epoxy and pristine CNT-epoxy composites were identical. Scanning electron microscopy (SEM) from both studies noted fiber pullout at the internal fracture surface as a common failure mode, which was indicative of a low CNT-epoxy interface strength [31,32]. Accordingly, Bie et al. also investigated functionalizing CNT surfaces for improved adhesion to the epoxy, however the spall strength was observed to decrease and was attributed to a change in the failure mechanism of the composite [32]. Similarly, Katz et al. [33] investigated the use of micron-scale fibers to reinforce an epoxy matrix, observing a drastic reduction in spall strength of the functionalized composite in comparison to the pristine fiber-reinforced composite. Strong matrix-filler adhesion would prevent the relaxation of thermal stresses, resulting in significant residual stresses that reduced the overall spall strength [33]. In a recent study of neat and halloysite nanotube-reinforced polyurethanes, Aguiar et al. [34,35] noted the role of the functionalized nanotubes participating in the polymerization process, leading to a refinement of the polymer microstructure that resulted in an improved spall strength of the polymer. Aguiar et al. [34,35] presented a markedly different concept of particle reinforcement, where the chemical processes in the polymerization reaction were altered by the presence of the nanotubes and the improvement in spall strength was not attributed to the nanotubes themselves. Thus, particle reinforcement may result in a competition between the standard void nucleation mechanisms and changes to the polymer microstructures.

The purpose of this study was to directly investigate the influence of particle morphology and matrix-particle interface adhesion on the spall strength of particle-reinforced polymer matrix composites. The model system used in this investigation was a polyurethane matrix reinforced with micron-scale alumina particles. Using silane functionalization of the alumina particle surfaces, the adhesion between the matrix and particles could be varied. The investigations included two morphologies of alumina particles and spall testing was conducted using a plate impact experiment.

2. Experimental details

The matrix material selected for the present study was a commercial thermoset polyurethane sold under the tradename Clearflex 95 (Smooth On). The particle reinforcement used in the present study was alumina (Panadyne), which was sourced in two different morphologies, spherical (Fig. 1a) and irregular (Fig. 1b). Both particle types had a nominal mean characteristic lengthscale of 5μm. All particle-reinforced composites in the present study had a fixed particle-phase volume fraction of 20%. In total, five sample types were prepared: (*i*) a baseline neat polyurethane; (*ii*) polyurethane reinforced with pristine spherical alumina; (*iii*) polyurethane reinforced with pristine irregular alumina; (*iv*) polyurethane reinforced with spherical alumina particles subjected to an adhesion-impeding silane-functionalization; and (*v*) a polyurethane silane blend. Each set of particles was sourced from the same batch from the manufacturer and each sample type was prepared from a single batch.

2.1. Preparation of materials

Prior to integration, the alumina particles were dried in an oven at 180°C for twelve hours to remove any moisture, allowed to cool, then stored in a nitrogen purged container to maintain a desicated state. To prepare the particle-reinforced composites, alumina was added at an appropriate mass fraction that was calculated to achieve a 20% volume fraction in the final composite. The alumina was added evenly to each part of the two-part polyurethane resin and mixed with a magnetic stirrer for 5 mins. An ultra-sonic probe mixer (Fisher Scientific FB 505) was used to thoroughly mix each suspension. A pulse cycle of 20 s on: 10 s off was used at 70% amplitude for a period of 5 minutes. After being allowed to cool, the two parts were combined and mixed via magnetic stirrer for 4 minutes. The mix was poured into open-faced moulds and degassed under vacuum for 4 minutes, after which point any remaining bubbles or foam were manually removed. Samples were then cured at room temperature for 6 hours, followed by a post-cure in an oven at 72°C for 16 hours. After being allowed to cool, samples were removed from their moulds.

One set of samples was prepared to impede the surface adhesion of the alumina particles to the polymer matrix. For these samples, the alumina particles were subjected to an adhesion-impeding silane-functionalization of the alumina particles prior to integration into the polyurethane matrix. Interface adhesion between the polymer and ceramic phases was tailored using a silane, n-octyltriethoxysilane (SIO6715.0 - Gelest), which was selected to suppress or impede adhesion. It was anticipated that the addition of this specific silane as a functionalizing agent would bonds to the active alumina surface and

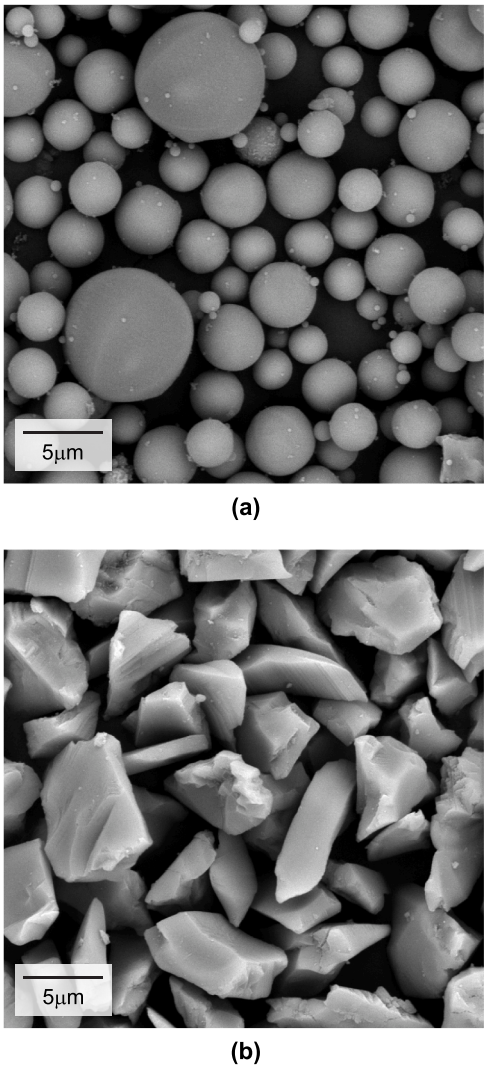

Fig. 1. SEM images of the (a) spherical and (b) irregular alumina particles.

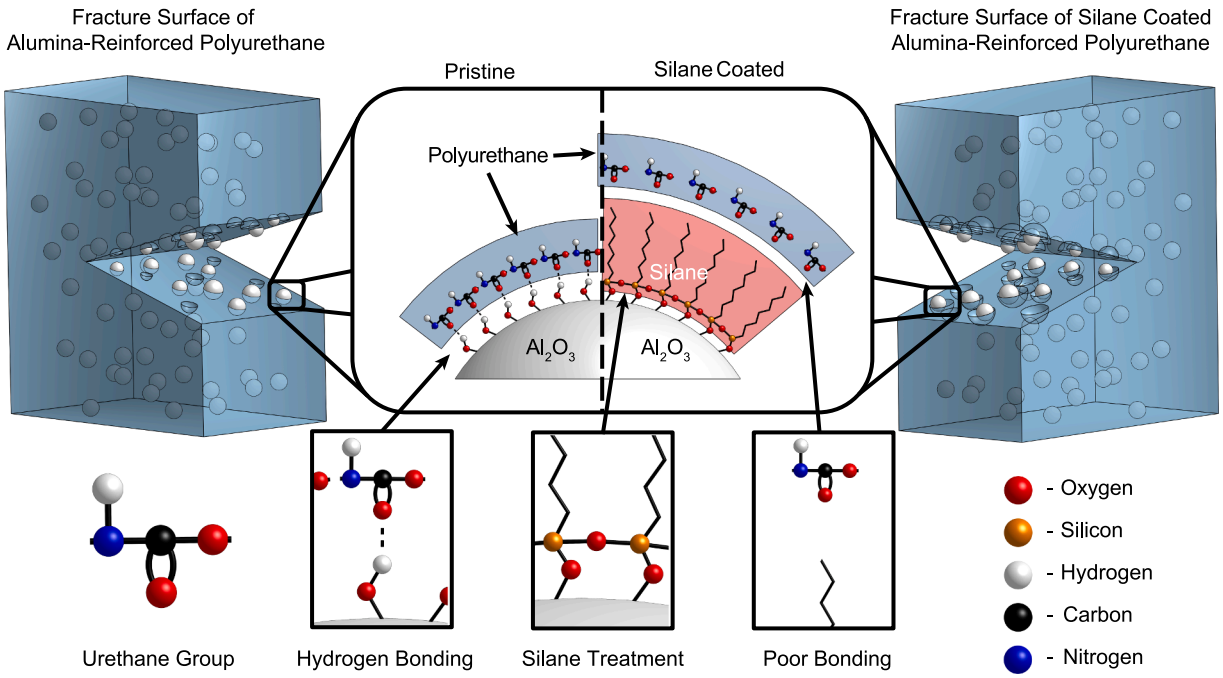

Fig. 2. A schematic demonstrating the effect of the silane on the surface adhesion of the spherical alumina particles.

present a less reactive aliphatic group to the polyurethane. This is shown schematically in Fig. 2.

A silane mass fraction of 5% (with respect to the alumina particles) was selected based on a literature survey of silane treatments of filler materials [36,37]. The silane treatment was applied to the dried alumina particles using the following technique. The silane was diluted in ethanol at a 1:2 ratio by mass and then mixed with the alumina. For every 100 g of alumina particles, 5 g of silane and 10 g of ethanol were used. Once coated, an additional 40 g of ethanol was added to the solution. An ultra-sonic probe mixer (Fisher Scientific FB 505) was used to thoroughly mix the solution. A pulse cycle of 20 s on: 10 s off was used at 70% amplitude for a period of 5 minutes. The mixture was then placed in an oven at 60°C overnight to evaporate the ethanol. The silane-functionalized alumina particles were then added to the polyurethane matrix following the procedure described above to prepare samples for testing. This silane treatment was only applied to spherical alumina particles.

Once the samples were cured, the density and sound speed of each sample type were determined experimentally. The density of each sample type was measured using four specimens from the same batch and the scatter is reported in Table 1. The longitudinal sound speed was determined using a pulse echo transducer (Olympus Technologies MG45) and a M202-RM linear transducer at a frequency of 10 MHz. A summary of the density and sound speed measurements for the samples investigated are shown in Table 1.

Table 1
Summary of the measured density and longitudinal sound speed for each sample type used in the present investigation.

Sample	Density (g/cm^3)	Sound Speed(m/s)
Neat Polyurethane	1.09 ± 0.03	2170 ± 10
Spherical Al_2O_3	1.66 ± 0.04	2090 ± 10
Irregular Al_2O_3	1.69 ± 0.04	2060 ± 10
Silane-Treated Al_2O_3	1.60 ± 0.04	1990 ± 20
PU + Silane Blend	1.09 ± 0.03	2020 ± 10

2.2. Plate impact testing

Plate impact testing was used to investigate the dynamic tensile (spall) strength of the various particle-reinforced polymer samples. The tests were conducted with a 67 mm internal diameter smooth-bore single-stage gas gun. Thin flyer plates were launched onto the samples at speeds ranging from 270 to 580 m/s. The instrumented samples were mounted in a machined target assembly (Fig. 3a) affixed with a small offset to the end of the barrel to ensure planarity of the mounted target

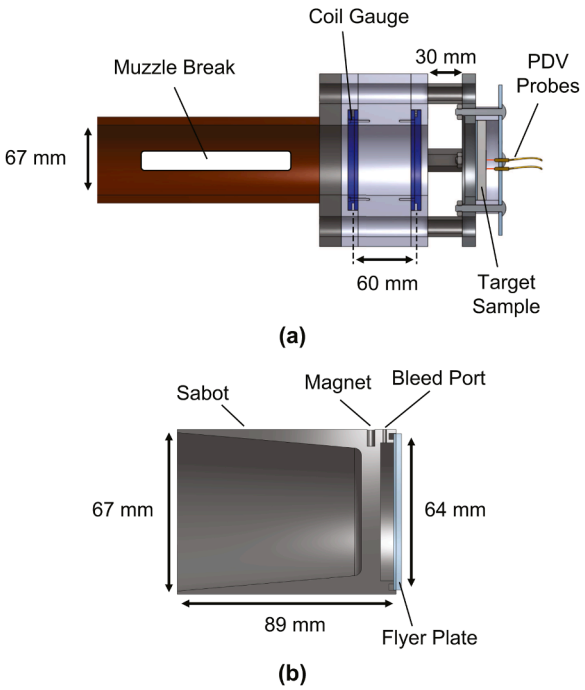

Fig. 3. Schematics of (a) the spall target assembly and diagnostics at the muzzle and (b) the flyer plate and sabot assembly.

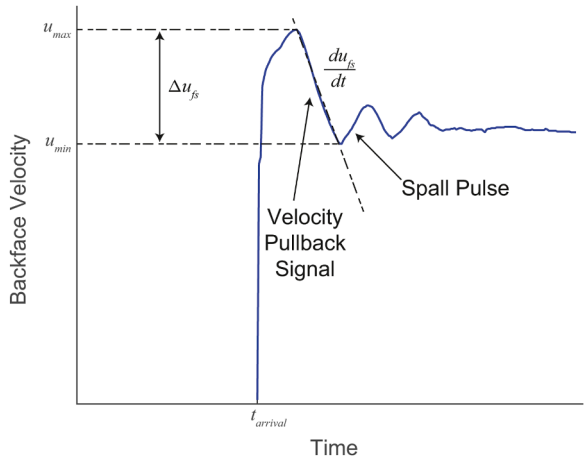

Fig. 4. An experimental backface velocity history from a spall test with labelled elements for data analysis.

with respect to the projectile. An 89 mm long PVC sabot supported a 64 mm diameter by 3.3 mm thick flyer plate with an air pocket immediately behind it, a schematic of which is shown in Fig. 3b. A combination of aluminum and acrylic flyer plates were used to achieve different loading conditions. A magnet was embedded within the sabot sidewall and used in conjunction with a stationary pair of annular induction coil gauges to determine the flyer plate velocity immediately prior to impact. The uncertainty in the coil gauge system was previously determined through a series of experiments comparing the exit velocity of projectiles measured by the PDV system and coil gauges concurrently. The uncertainty in the coil gauges measurements was determined to be on the order of 1.5% of the measured speed [38]. The gun barrel and test chamber were evacuated to a pressure of approximately 100 Pa prior to firing the projectile. The target material sample thicknesses (w_t) varied between 4.5 and 11.2 mm.

The target material samples were instrumented with a two-channel photonic Doppler velocimeter (PDV) to monitor the backface velocity history of the test material [39,40]. The backface velocity history of the rear free surface of the target materials can be related to the mechanics of the wave processes occurring within the target material, which can be related to the spall failure strength of the samples [41]. A 50-μm-thick piece of aluminized Mylar foil was adhered to the back face of each sample using cyanoacrylate to serve as a reflector for a PDV laser collimator probe. Two PDV probes were placed on a common radius from the centre of the sample for redundancy. The PDV system recorded the signal with a peak bandwidth of 12.5 GHz and was sampled at a rate of 40 GS/s.

2.3. Analysis of plate impact data

The spall strengths of the material samples were determined from the velocity history measured in the experiments (Fig. 4). These values were calculated using an acoustic approach [41] to relate spall strength to the pullback velocity according to the equation,

$$\sigma^* = \frac{1}{2}\rho_0 C_0 \Delta u_{fs}, \tag{1}$$

where ρ_0 is density, C_0 is bulk sound speed, and Δu_{fs} is the difference between the peak and pullback free surface velocity of the sample. As we were unable to obtain reliable shear wave velocities for these polymers, the bulk sound speed will be approximated by the measured longitudinal sound speeds (Table 1). The experimental strain rate ($\dot{\varepsilon}$) relating to the spall event can also be measured from the velocity history based on the rate of backface unloading in the target material,

$$\dot{\varepsilon} \approx \frac{1}{2 \cdot C_0} \frac{du_{fs}}{dt}. \tag{2}$$

Table 2
Summary of the results from the plate impact tests.

(mm)	Target	w_t (mm)	w_f (m/s)	V_{Flyer} (m/s)	Flyer Material	u_{peak} (m/s)	u_{pull} (MPa)	σ_{spall} ($10^4 s^{-1}$)	$\dot{\varepsilon}$
1 - Neat PU	8.4	3.3	431	Acrylic	471.0 446.9	327.6 307.4	167 ± 2	3.0	
2 - Neat PU	8.4	3.3	292.1	Acrylic	317.7	165.30	180 ± 2	2.4	
3 - Neat PU	8.2	3.3	290.4	Acrylic	275.1	122.7	180 ± 2	2.5	
4 - Neat PU	8.1	3.3	286	Aluminum	417.2	266.1	179 ± 2	1.8	
5 - Neat PU	3.6	3.3	291	Acrylic	334.8	192.2	169 ± 2	3.4	
6 - Neat PU	4.0	3.3	287	Acrylic	318.8	172.0	174 ± 2	3.4	
7 - PU + Sph. Al_2O_3	11.1	3.3	437	Acrylic	417.2	316.5	175 ± 9	1.9	
8 - PU + Sph. Al_2O_3	8.9	3.3	292	Acrylic	251.9 251.9	158.9 152.4	167 ± 6	1.6	
9 - PU + Sph. Al_2O_3	8.7	3.3	576	Acrylic	532.2 517.0	403.0 404.0	210 ± 14	2.0	
10 - PU + Sph. Al_2O_3	8.8	6.4	287	Acrylic	259.6	147.2	195 ± 10	0.9	
11 - PU + Irr. Al_2O_3	8.7	3.3	439	Acrylic	356.5 378.5	266.1 285.5	160 ± 2	1.6	
12 - PU + Irr. Al_2O_3	8.7	3.3	286	Acrylic	210.5	95.6	201 ± 3	1.5	
13 - PU + Irr. Al_2O_3	9.2	3.3	412	Acrylic	436.6 427.0	344.9 333.2	162 ± 2	1.1	
14 - PU + Silane + Sph. Al_2O_3	4.5	3.3	427	Acrylic	422.6 412.3	383.0 380.3	57 ± 6	2.2	
15 - PU + Silane + Sph. Al_2O_3	4.8	3.3	402	Acrylic	382.0 382.8	356.5 360.0	38 ± 2	1.6	
16 - PU + Silane + Sph. Al_2O_3	5.1	3.3	403	Aluminum	603.5	566.0	60 ± 4	3.8	
17 - PU + Silane + Sph. Al_2O_3	10.2	3.3	548	Acrylic	487.2 471.2	433.5 424.2	81 ± 5	1.9	
18 - PU + Silane Blend	8.7	3.3	281	Aluminum	436.1	280.0	172 ± 1	3.1	
19 - PU + Silane Blend	8.2	3.3	290	Acrylic	311.7 303.1	163.6 153.3	159 ± 1	2.7	

3. Results

A total of 19 experiments were conducted for the present study, the test parameters and results from which are summarized in Table 2. Those experiments with multiple PDV probe measurements list both sets of data and an average spall strength and strain rate. The uncertainty in the spall strengths of a given experiment were determined from the variations seen among the two PDV probes monitoring the same experiment. The uncertainty among samples for which only one PDV probe measurement was available was estimated as the average multi-probe scatter measured in other samples of the same type. The average uncertainty values estimated from the experiments were approximately 4% of the measured strengths. This method of estimating PDV uncertainty was similar to the approach of Farbaniec et al. [42].

The backface velocity histories are shown in Fig. 5 and the results from all of the materials tested are plotted against strain rate in Fig. 6. Many of the free surface velocity histories in Fig. 5 show a showed a sharp jump associated with wave arrival and a slow rise to peak amplitude. This is characteristic of the visco-elastic response of these materials [43,44].

There are several trends that were immediately apparent from the datasets (Fig. 6). The first observation was that despite the addition of alumina particles, when they were in their pristine form, the spall strength of the composite was indistinguishable from failure strength of the neat polyurethane matrix. The scatter in the data becomes more significant however the mean value was unchanged. The results also showed that the morphology of the particles was not an important factor in the failure strength of the composite, as both irregular and spherical particles had the same spall strengths. The significant change in spall strength was seen for the spherical alumina particles that were treated with an adhesion-impeding silane-functionalization prior to integration into the composite. This was a significant drop in strength, which appears to be related to the change in the surface chemistry of the particles.

Out of concern that the change in spall strength was due to the silane interfering with the chemistry of the polymer matrix, two samples were cast with a polyurethane and silane blend, where the silane was present with the identical silane to polymer volume fraction as in the silane-functionalized particle systems. The spall strength of the polyurethane-silane blend was unchanged from the values measured in the neat polyurethane (Fig. 6).

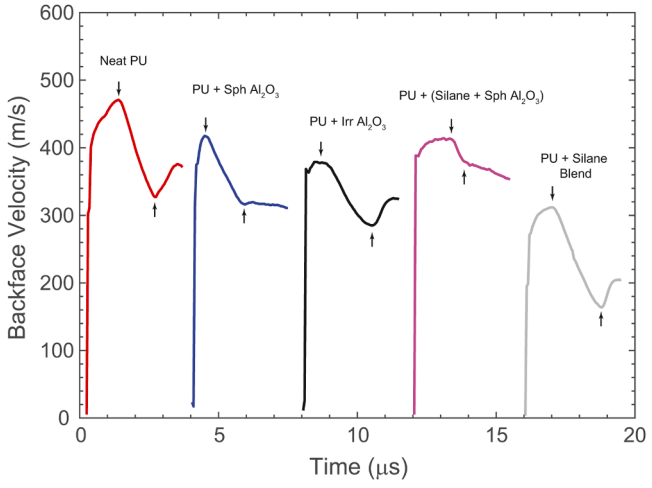

Fig. 5. A sample of the typical backface velocity histories measured for each sample type. The time axis of the signals have been arbitrarily shifted for visualization purposes. The arrows indicate the chosen peak and pull-back velocities.

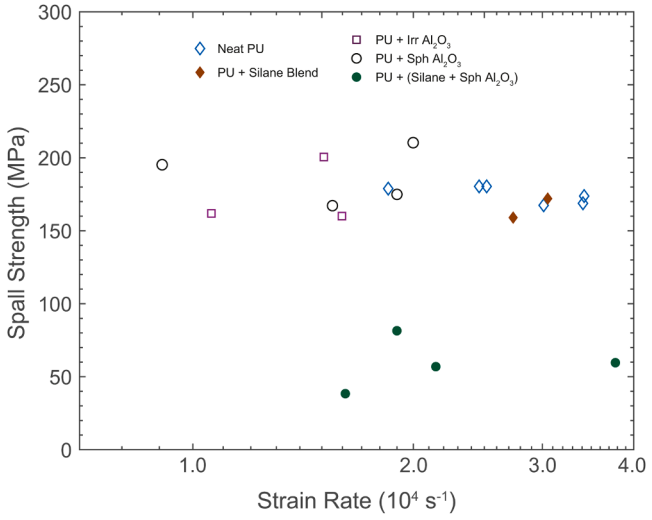

Fig. 6. Experimental spall strength for the five samples against strain rate.

4. Discussion

The spall strengths measured for neat polyurethane, which ranged between 167–180 MPa, were consistent with previously reported values for different polymers, which often range between 100–200 MPa [18,30,43]. These spall strengths are one order of magnitude higher than the quasi-static tensile strength (17 MPa) quoted by the manufacturer. This increase was consistent with Ree-Eyring theory [45], which suggests a strengthening response due to a restricted molecular mobility at high strain rates, as well as the results of previous work on epoxy [30].

4.1. Effect of particle reinforcement on spall strength

From Fig. 6, it is clear that the addition of alumina particles into polyurethane resulted in no discernible change in the spall strength of the composite. These results stand in contrast to prior work on the presence of second phase particles in other material systems, which has been shown to reduce spall strength of a material in both metals [25,26] and polymers [31]. In these cases, the onset of spall is typically attributed to the matrix-filler interface behaving as a preferential site for void nucleation, due to poor matrix-filler adhesion in polymers [31,46] and debonding at secondary phase boundaries [25]. These results would suggest that adhesion between the pristine alumina particles and the polyurethane matrix is strong, a fact that has been noted in prior studies on similar polymeric material systems [47,48] as well as in metals [28]. Strong matrix-filler adhesion would likely suppress the preferential nucleation of voids at the particle-matrix.

4.2. Effect of particle morphology

Two particle morphologies of the alumina particles integrated into the polyurethae were investigated in the present work, spherical and irregular morphologies; however, there was no discernable difference in the spall strength of these two polymer composites (Fig. 6). It was anticipated that the composites with particles having irregular morphologies would outperform the composites with spherical particles based on prior dynamic fracture experiments on particle-reinforced epoxy [49] and quasi-static and ballistic data on particle-reinforced elastomers [48]. Those prior studies had found that fillers having higher aspect ratios outperformed comparable filler volumes with lower aspect ratios, which were explained in terms of differences in energy dissipation [49] and elastomer mobility [48].

The similarity in spall strengths between the irregular and spherical alumina composites reinforce the hypothesis that the failure of these samples was dominated by void nucleation at the particle-matrix interface. At the elevated volume fractions investigated in the present

study, spall failure was not limited by interface density, thus void nucleation densities would have been similar. Recent results on spall behaviour in silicon oils [50] observed that the presence of pre-existing bubbles in silicon oil did not reduce its spall strength. While this may similarly seem counter intuitive, this was attributed to the fact that randomly formed bubbles within the oils served as sufficiently favourable nucleation sites. Having an abundance of nucleation site candidates in both composite samples, spall behaviour was likely energy limited. Since the applied energy is comparable, regardless of particle morphology, the nucleation of voids depends primarily on the adhesion at the particle-matrix interface.

4.3. Silane-Treated composite samples

As a means of interrogating the hypothesis surrounding the role of particle surface adhesion on the spall failure of particle-matrix composites, an adhesion-impeding silane functionalization was used to coat the particles prior to their integration within the polymer matrix. As the adhesion between alumina and polyurethane was determined to be sufficiently strong, the functionalization was used as a means of suppressing this adhesion. From Fig. 6, the silane functionalization of the particles resulted in a significant drop in spall strength, in comparison to both neat polyurethane and the composite with the pristine particles. These results showed a substantial drop, which is directly attributable to the change in particle surface chemistry reducing the particle-matrix adhesion at the interface.

As a further note, identifying the pullback velocity for polymer materials undergoing spall can be difficult. For example, comparing two of the backface velocity histories in Fig. 5, one from the pristine particles and the other from the silane-treated particles, the spall pulse signals differ significantly. This can be attributed to the dispersion of the compression waves generated at the spall plane [31]. These types of spall pulse signals are commonly seen in a variety of polymers and have lead to significant scatter between reported results, as the choice of pullback velocity was not clear. For the silane-treated samples, the spall pulse had two characteristic values that could be considered when calculating the spall strength, which can be seen as an inflection point in the unloading and the local minimum of the velocity history.

In the present study, the inflection point was determined to be the suitable pullback velocity for two primary reasons: the strain rate of the material pre- and post-inflection and the timing of the internal wave interactions. The most compelling reason to choose the inflection point as the true onset of spall, is that the strain rates prior to the inflection point were on the order of $10^4\ s^{-1}$, which was consistent with every other material tested, while the strain rate post-inflection was on the order of $10^3\ s^{-1}$. Given that the silane treated samples were thinner than the pristine samples (see Table 2), the strain rates were expected to be higher in the silane-treated samples. A second consideration is the amount of time required for the silane treated samples to unload and spall. A simple estimate for a silane-treated sample struck at 400 m/s, predicts a free surface velocity plateau with a duration of ≈ 1.5 μs, prior to the arrival of the leading edge of the rarefaction rarefaction fan. The tailing edge of the fan arrives about 1 μs after that, based on the measured speed of sound. Since spall relies on the interaction of rarefaction fans to generate a tensile state, spall would occur prior to the arrival of the tailing edge of the rarefaction fan. The above described inflection point lies within this one microsecond window, while the minimum point of the free surface spectrogram is seen almost 4 μs after the onset of unloading. This suggests one should use the inflection point in the velocity history as the pullback velocity.

With the drastic reduction in spall strength with the integration of silanes into these composites, there was some concern that the silane itself may be interfering with the polymerization of the polyurethane. To discount this possibility, a polyurethane-silane blend to the same ratio seen in the adhesion-impeding silane-treated composites. As can be seen in Fig. 6 and Table 2, a negligible difference was observed in the spall strength and physical properties of the neat polyurethane and polyurethane-silane blend. This implies the silane alone has a minimal effect on the overall chemistry of the polyurethane, suggesting that differences seen in the composite treated for negative adhesion can be attributed to impeded interface adhesion. Furthermore, the backface velocity histories of the neat polyurethane and polyurethane-silane blend shown in Fig. 5, suggests that the silane did not impede the polymerization of the neat polyurethane.

Reviewing the results of the spall testing listed in Table 2 and shown in Fig. 6, it is clear that impeding the interface adhesion between the alumina and polyurethane resulted in a drastic reduction in dynamic tensile strength. The stronger interface adhesion in the untreated composite benefits the overall composite by behaving as a less suitable candidate for spall nucleation. As per the energy-limited and flaw-limited theories [22,51], this would suggest that more energy is expended in developing the interface, so that it can behave as a suitable nucleation site. On the contrary, the silane-treated composite is likely to behave as an excellent candidate site for spall nucleation, as the low strength interface would possess little strength to resist void nucleation.

4.4. Fracture surface analysis

Several samples were recovered from the spall experiments for a qualitative analysis of their fracture surfaces using a Scanning Electron Microscope (SEM). The recovered samples were carefully sectioned along their spall plane and sputter-coated with a 10 nm layer of gold. Two SEM images of fracture planes are shown in Figs. 7a and 7b for pristine and silane coated spherical alumina particles, respectively.

The micrographs in Fig. 7 captured several features that deserve attention. The first observation is that both images showed evidence of

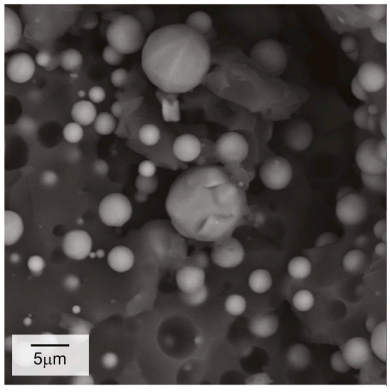

(a)

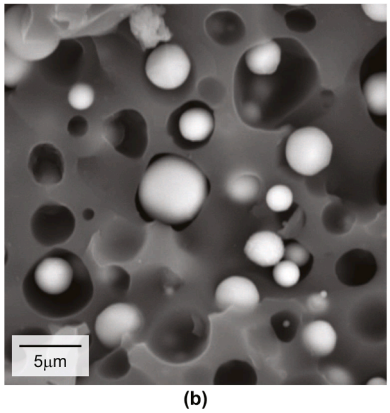

(b)

Fig. 7. SEM images displaying the fracture surface of a spherical alumina reinforced PU sample.

particle pullout for the two particle composites. The two images show a number of pockets remaining where a spherical alumina particle was pulled out of the matrix under the applied dynamic tensile load, as well as several exposed particle surfaces that were pulled out of the adjoining matrix material prior to fracture. This was to be expected, as the alumina particles are extremely hard and were not expected to fracture under these loading conditions.

A second, more nuanced, observation that can be made from these micrographs is that while both composites feature well-dispersed particle phases, there is a notable difference in the surface wetting of the particles in the two composites. The pristine alumina particles in Fig. 7a appear to have bonded well to the matrix with excellent surface wetting. In contrast, the adhesion-impeding silane-functionalization of the particles in Fig. 7b appeared to have created a poorly wetted particle surface, as one would expect. These images visually demonstrate that the silane treatment did reduce the adhesion of the particle surface to the polyurethane matrix, as intended. These gaps were a consequence of the silane treatment applied to the particles prior to integration. These gaps at the particle-matrix interface would readily behave as preferential void nucleation sites within the composite. Since particle pullout is common in both materials, the reduction in particle wetting, and thus adhesion, caused a drastic reduction in the spall strength of the silane-treated samples.

5. Conclusions

The objective of the present study was to assess the role played by particle morphology and matrix-filler interface adhesion on the spall strength of particle-reinforced polymer matrix composites. The addition of the pristine particles did not result in a change in spall strength as compared to the matrix material, regardless of particle morphology. In evaluating matrix-filler adhesion, a drastic reduction in spall strength was observed with a reduction in adhesion between the two phases. This reduction was attributed to a loss of adhesion at the particle surface with the addition of a silane surface treatment on the alumina particles, despite otherwise having an identical sample composition. From this, concerns of silane interference with the polymer matrix were eliminated showing a near identical behaviour and spall strength between the polyurethane and silane-polyurethane blend. Microscopy of the fracture surfaces of silane-treated and untreated particle composites corroborated the interpretation of the experimental spall strength measurements. The silane treatment reduced the wetting of particle surfaces, creating preferential nucleation sites for spall failure.

CRediT authorship contribution statement

Anton Lebar: Conceptualization, Methodology, Data curation, Formal analysis, Writing - original draft. **Rafaela Aguiar:** Methodology, Formal analysis. **Andrew Oddy:** Methodology, Data curation. **Oren E. Petel:** Conceptualization, Methodology, Writing - review & editing, Supervision.

Declaration of Competing Interest

The authors have no competing interests to declare in relation to this research.

Acknowledgements

This work funded through the financial support of the Natural Sciences and Engineering Research Council of Canada (NSERC) through the Discovery Grant program (RGPIN-2014-06295). The PDV system was purchased through the NSERC Research Tools and Instruments program (RTI-2019-00931).

References

[1] Grujicic M, Pandurangan B, Angstadt D, Koudela K, Cheeseman B. Ballistic-performance optimization of a hybrid carbon-nanotube/e-glass reinforced poly-vinyl-ester-epoxy-matrix composite armor. J Mater Sci 2007;42:5347–59.
[2] Pandya K, Akella K, Joshi M, Naik N. Ballistic impact behavior of carbon nanotube and nanosilica dispersed resin and composites. J Appl Phys 2012;112(11):113522.
[3] Sutherland H, Munson D. Stress wave propagation in a cloth-laminate carbon phenolic. J Compos Mater 1976;10(2):118128.
[4] Dandekar D, Boteler J, Beaulieu P. Elastic constants and delamination strength of a glass-fiber-reinforced polymer composite. Compos Sci Technol 1998;58(9):1397–403.
[5] Zaretsky PM, E DeBotton G. The response of a glass fibers reinforced epoxy composite to an impact loading. Int J Solids 2004;41(2):569–84.
[6] Millett J, Meziere Y, Bourne N. The response to shock loading of a glass-fibreepoxy composite: effects of fibre orientation to the loading axis. J Phys D 2007;40(17):5358.
[7] Tang LC, Zhang H, Wu XP, Zhang Z. A novel failure analysis of multi-walled carbon nanotubes in epoxy matrix. Polymer (Guildf) 2011;52(9):2070–4. https://doi.org/10.1016/j.polymer.2011.03.002.
[8] Naveen J, Jawaid M, Zainudin E, Sultan M, Yahaya R. Effect of graphene nanoplatelets on the ballistic performance of hybrid kevlar/cocos nucifera sheath-reinforced epoxy composites. Text Res J 2019;89(21–22):4349–62.
[9] Mock Jr W, Holt W. Shockwave compression of an aluminafilled epoxy in the low gigapascal stress range. J Appl Phys 1978;49(3):1156–8.
[10] Chhabildas L, Swegle J. On the dynamical response of particulateloaded materials. i. pressureshear loading of alumina particles in an epoxy matrix. J Appl Phys 1982;53(2):954–6.
[11] Setchell R, Anderson M. Shock-compression response of an alumina-filled epoxy. J Appl Phys 2005;97(8):083518.
[12] Setchell R, Anderson M, Montgomery S. Compositional effects on the shock-compression response of alumina-filled epoxy. J Appl Phys 2007;101(8):083527.
[13] Millett J, Deas D, Bourne N, Montgomery S. The deviatoric response of an alumina filled epoxy composite during shock loading. J Appl Phys 2007;102(6):063518.
[14] Neel C, Thadhani N. Shock and release wave speed of an alumina epoxy composite. J Appl Phys 2009;ournal of Applied Physics > Volume 106, Issue 4(4):046105.
[15] Vogler T, Alexander C, Wise J, Montgomery S. Dynamic behavior of tungsten carbide and alumina filled epoxy composites. J Appl Phys 2010;107(4):043520.
[16] Butcher BM, Barker LM, Munson DE, Lundergan CD. Influence of stress history on time-dependent spall in metals. AIAA J 1965;2(6):977–90. https://doi.org/10.2514/6.1963-232.
[17] Meyers MA, Taylor Aimone C. Dynamic fracture (spalling) of metals. Prog Mater Sci 1983;28(1):1–96. https://doi.org/10.1016/0079-6425(83)90003-8.
[18] Antoun T, Seaman L, Curran DR, Kanel GI, Razorenov SV, Utkin AV. Spall fracture. 1st. New York, NY: Springer; 2003. https://doi.org/10.1007/b97226.
[19] Nahme H, Lach E. Dynamic behavior of high strength armor steels. Le J Phys IV 1997;07(C3):C3–373–C3–378. https://doi.org/10.1051/jp4:1997365.
[20] Jones DR, Fensin SJ, Martinez DT, Trujillo CP, Gray GT. Effect of peak stress and tensile strain-rate on spall in tantalum. J Appl Phys 2018;124(8). https://doi.org/10.1063/1.5045045.
[21] Gray III G, Bourne N, BL H. On the influence of loading profile upon the tensile failure of stainless steel. J Appl Phys 2007;101(9):093507.
[22] Grady DE. Incipient spall, crack branching, and fragmentation statistics in the spall process. Le J Phys Colloq 1988;49(C3):C3–175–C3–182. https://doi.org/10.1051/jphyscol:1988326.
[23] Fensin SJ, Walker EK, Cerreta EK, Iii GTG. When do interfaces become important for failure? EPJ Web Conf 2015;94:2010. https://doi.org/10.1051/epjconf/20159402010.
[24] Appleby-Thomas GJ, Hazell PJ. A study on the strength of an armour-grade aluminum under high strain-rate loading. J Appl Phys 2010;107(12). https://doi.org/10.1063/1.3431346.
[25] Williams CL, Sano T, Walter TR, Bradley J, Kecskes LJ. The role of second phase intermetallic particles on the spall failure of 5083 aluminum. J Dyn Behav Mater 2016;2(4):476–83. https://doi.org/10.1007/s40870-016-0082-2.
[26] Appleby-Thomas GJ, Hazell PJ. A study on the strength of an armour-grade aluminum under high strain-rate loading. J Appl Phys 2010;107(12):1–12. https://doi.org/10.1063/1.3431346.
[27] Wang W, Zhang H, Yang M, Jiang P, Yuan F, Wu X. Shock and spall behaviors of a high specific strength steel: effects of impact stress and microstructure. J Appl Phys 2017;121(13). https://doi.org/10.1063/1.4979346.
[28] Hixson RS, Johnson JN, Gray GT, Price JD. Effects of interfacial bonding on spallation in metal-matrix composites. AIP Conf. Proc. 370. AIP; 1996. p. 555–8. https://doi.org/10.1063/1.50872.
[29] Fensin S, Walker E, Cerreta E, Trujillo C, Martinez D, Gray III G. Dynamic failure in two-phase materials. J Appl Phys 2015;118:235305.
[30] Pepper JE, Huneault J, Rahmat M, Ashrafi B, Petel OE. The effect of curing agent on the dynamic tensile failure of an epoxy subjected to plate impact. Int J Impact Eng 2018;113:203–11. https://doi.org/10.1016/j.ijimpeng.2017.11.009.
[31] Huneault J, Pepper JE, Rahmat M, Ashrafi B, Petel OE. Spall characterization of EPON 828 epoxy with embedded carbon nanotubes. J Dyn Behav Mater 2019;5(1):13–23. https://doi.org/10.1007/s40870-018-00180-w.
[32] Bie BX, Han JH, Lu L, Zhou XM, Qi ML, Zhang Z, et al. Dynamic fracture of carbon nanotube/epoxy composites under high strain-rate loading. Compos Part A Appl Sci Manuf 2015;68:282–8. https://doi.org/10.1016/j.compositesa.2014.10.001.

[33] Katz S, Zaretsky E, Grossman E, Wagner HD. Dynamic tensile strength of organic fiber-reinforced epoxy micro-composites. Compos Sci Technol 2009;69(7–8): 1250–5. https://doi.org/10.1016/j.compscitech.2009.02.031.
[34] Aguiar R, Miller R, Petel O. Synthesis and characterization of partially silane-terminated polyurethanes reinforced with acid-treated halloysite nanotubes for transparent armour systems. Sci Rep 2020;10(1):13805.
[35] Aguiar R, Lebar A, Oddy A, Miller R, Petel O. Synthesis and mechanical characterization of polyurethane reinforced with halloysite nanotubes. AIP Conference Proceedings 2020;2272(1):120001. https://doi.org/10.1063/12.0001015.
[36] Zhang Y, Park SJ. Effect of mercapto-Terminated silane treatment on rheological and mechanical properties of rice bran carbon-Reinforced nitrile butadiene rubber composites. Macromol Res 2018;26(5):446–53. https://doi.org/10.1007/s13233-018-6058-3.
[37] Ishak ZAM, Aminullah A, Ismail H, Rozman HD. Effect of silane-Based coupling agents and acrylic acid based compatibilizers on mechanical properties of oil palm empty fruit bunch filled high-Density polyethylene composites. J Appl Polym Sci 1997;68:2189–203. https://doi.org/10.1002/(SICI)1097-4628(19980627)68:13<2189::AID-APP16>3.0.CO;2-V.
[38] Lebar A. A Study of Particle Surface Effects on the Spall Strength of Particle-Reinforced Polymer Matrix Composites. Carleton University; 2020. Masc.
[39] Strand OT, Goosman DR, Martinez C, Whitworth TL, Kuhlow WW. Compact system for high-speed velocimetry using heterodyne techniques. Rev Sci Instrum 2006;77 (8):083108. https://doi.org/10.1063/1.2336749.
[40] Dolan D. Extreme measurements with photonic doppler velocimetry (PDV). Rev Sci Instrum 2020;91:051501.
[41] Novikov SA, Ivanov AG. Failure of steel, aluminium and copper under explosive shock loading. Fiz Met-i Metalloved 1966;21(4):608–15.
[42] Farbaniec L, Williams CL, Kecskes LJ, Becker R, Ramesh KT. Spall response and failure mechanisms associated with a hot-extruded AMX602 mg alloy. Mater Sci Eng A 2017;707(June):725–31. https://doi.org/10.1016/j.msea.2017.09.105.
[43] Curran DR, Shockey DA, Seaman L. Dynamic fracture criteria for a polycarbonate. J Appl Phys 1973;44(9):4025–38. https://doi.org/10.1063/1.1662891.
[44] Johnson JN. Spallation studies in Estane. AIP Conf. Proc. 505. AIP; 2000. p. 543–6. https://doi.org/10.1063/1.1303532.
[45] Ree T, Eyring H. Theory of non-Newtonian flow. i. solid plastic system. J Appl Phys 1955;26(7):793–800.
[46] Pepper JE, Huneault J, Rahmat M, Petel OE. Spall strength measurements in EPON 828 epoxy and an epoxy/carbon nanotube composite. AIP Conf. Proc. 1979; 2018, ISBN 9780735416932. p. 070024. https://doi.org/10.1063/1.5044833.
[47] Lebar A, Oddy A, Aguiar R, Petel O. Effect of interface adhesion on the spall strength of particle-reinforced polymer matrix composites. AIP Conference Proceedings 2020;2272(1):120012. https://doi.org/10.1063/12.0000781.
[48] Comtois-Arnaldo C. The Ballistic Response of Particle-filled Elastomeric Systems. Carleton University; 2018. Masc.
[49] Kushvaha V, Tippur H. Effect of filler particle shape on dynamic fracture behavior of glass-Filled epoxy. Conf. Proc. Soc. Exp. Mech. Ser. 4; 2013. p. 513–22. https://doi.org/10.1007/978-1-4614-4238-7_66.
[50] Huneault J, Higgins AJ. Shock wave induced cavitation of silicone oils. J Appl Phys 2019;125(24):1–11. https://doi.org/10.1063/1.5093028.
[51] Grady D. The spall strength of condensed matter. J Mech Phys Solids 1988;36(3): 353–84. https://doi.org/10.1016/0022-5096(88)90015-4.